Research Article

Fatimah Ali M. Al-Zahrani* and Reda M. El-Shishtawy

Green synthesis and characterisation of spherical structure $Ag/Fe_2O_3/TiO_2$ nanocomposite using acacia in the presence of neem and tulsi oils

https://doi.org/10.1515/gps-2023-0218
received October 25, 2023; accepted March 7, 2024

Abstract: In this study, tulsi and neem oils were used to effectively synthesise $Ag/Fe_2O_3/TiO_2$ nanocomposite utilising environmentally friendly methods. X-ray diffraction analysis (XRD), scanning electron microscopy (SEM), energy-dispersive X-ray spectroscopy, and Fourier-transform infrared spectroscopy (FT-IR) methods were used to characterise the green synthesised nanocomposite. The triangle-spherical shaped nanoparticles (NPs) with an average size of 26–42 nm were shown by XRD and SEM investigations to be crystalline in $Ag/Fe_2O_3/TiO_2$ nanocomposite, respectively. Additionally, the dynamic light scattering histogram was used to quantify the size distribution of these NPs, and the results were consistent with those of the SEM picture, having an approximate element size of 28 nm. The $Ag/Fe_2O_3/TiO_2$ nanocomposite is reduced and stabilised as a result of functional groups present in acacia, and neem, and tulsi oils, as shown by FT-IR measurements. In a nutshell, this method offers a quick, affordable, and environmentally safe technique to create NPs without the use of potentially dangerous chemical agents.

Keywords: tulsi oil, neem oil, $Ag/Fe_2O_3/TiO_2$ nanocomposite, characterisation, green synthesis

1 Introduction

Biosynthesis of nanomaterials using medicinal plant oils has received much attention in recent years. The synthesis of nanomaterials by medicinal plant oils is more environmentally friendly and cost-effective than other synthesis methods, such as chemical reduction and physical methods [1,2]. Biosynthesis of nanomaterials has gained attention as an emerging feature of the interface between nanotechnology and biotechnology due to the increasing demand for environmentally friendly material manufacturing techniques [3]. The biosynthesis of inorganic materials, especially metal nanoparticles (NPs), using microbes and plants has received great attention [4–6]. "Green" synthesis strategies include the use of non-toxic materials, hazardous chemicals, biodegradable polymers, and eco-friendly solvents such as plant extracts These methods use extracts from various plant parts, microbial cells, and biopolymers, and are thus classified as green synthesis methods. The essential benefit of using plant extracts as biogenic sources of metallic synthesis is because they accelerate the reduction and stability of the NPs at room temperature and pressure (e.g., [7–9]). Due to its reputed therapeutic properties, tulsi (Ocimum sanctum), or Holy basil, from the family Lamiaceae, has been referred to as the "Queen of plants" and the "mother medicine of nature" [10]. Almost every component of the plant has been shown to have medicinal effects, making it one of the most revered and all-encompassing herbs utilised in Indian traditional medicine over the years [11]. Since Ocimum sanctum is used in several ways in traditional medicine; aqueous extracts from the leaves (naturally picked or even dried) are added to herbal teas or blended with various types of other herbs or honey to increase their therapeutic potency. Aqueous extracts of Tulsi have long been used to treat a variety of poisonings, stomach-aches, migraines, the parasite malaria, chronic inflammation, as well as heart conditions [12]. As medicines, painkillers, anti-emetics, antipyretics, stress relievers, inflammatory agents, as well as hepatoprotective, anti-asthmatic, hypoglycaemic, hypotensive, hypolipidemic, and immuno-modulatory agents, oils obtained from Ocimum sanctum as well as its leaves are considered to have a number of beneficial properties [12,13]. Due to the presence of vital or essential oil, which is mostly concentrated in the leaf of tulsi, the plant has a distinctive fragrant scent. The primary constituents of this aromatic volatile oil include phenols, terpenes, and aldehydes [14]. Fixed oil is the term for the

* **Corresponding author: Fatimah Ali M. Al-Zahrani,** Chemistry Department, Faculty of Science, King Khalid University, Abha 61413, Saudi Arabia, e-mail: falzhrani@kku.edu.sa
Reda M. El-Shishtawy: Chemistry Department, Faculty of Science, King Abdulaziz University, Jeddah, 21589, Saudi Arabia; Dyeing, Printing and Textile Auxiliaries Department, Textile Research Division, National Research Centre, Dokki, Cairo, Egypt

oil that is derived from seeds and is mostly made up of fatty acids. The plant also has alkaloids, glycosides, saponins, and tannins in addition to oil. The leaves also contain carotene and ascorbic acid [15,16]. Figure 1 displays the specifics of the chemical components described in several publications.

The neem tree (*Azadirachta indica* Juss), a member of the Meliaceae family that originated in India and is today regarded as a significant resource of phytochemicals which is effectively utilised not only in human health but also in pest management, is used to extract neem oil [17]. A small to medium evergreen tree with broad and spreading branches, *Azadirachta* grows quickly. Both high temperatures and weak or deteriorated soil are acceptable to it. The mature leaves, which have a brilliant green petiole, lamina, and the base that connects the leaf to the stem, are reddish to purple in colour in contrast to the young leaves' reddish to purple hues [18].

A minimum of 100 physiologically active substances can be found in neem oil [19]. Triterpenes known as limonoids, the most significant of which is azadirachtin (Figure 1), are among their main ingredients and are thought to be responsible for 90% of the action on most pests [20]. The substance has a molecular weight of 720 $g \cdot mol^{-1}$ and a melting point of 160°C. Nimbidin, meliantriol, nimbin, nimbolides, fatty acids (oleic, stearic, and palmitic), and salannin are also included [21,22]. The oil obtained by various methods from the seeds is the primary neem product. Although the other neem tree sections are utilised to extract oil, they do not have as much azadirachtin [23]. It has been proposed that artificial inoculation with arbuscular mycorrhiza can enhance the amount of azadirachtin in seeds [24] (Figure 2).

Iron oxide has numerous advantages, including a narrow band gap energy of about 2.2 eV, low cost, non-toxicity, availability, and thermal stability. Magnetite contains both ferrous

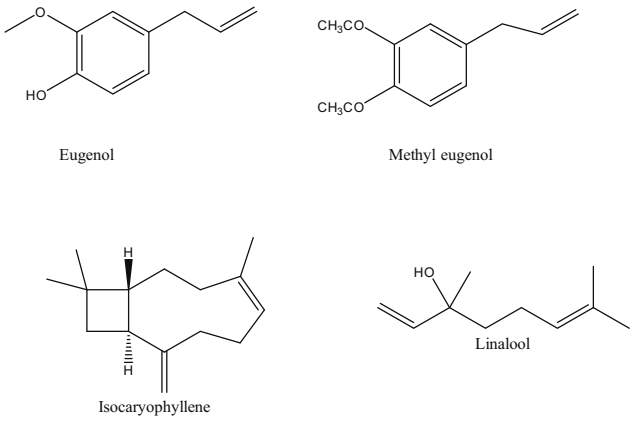

Figure 1: Chemical constituents of *Ocimum sanctum*.

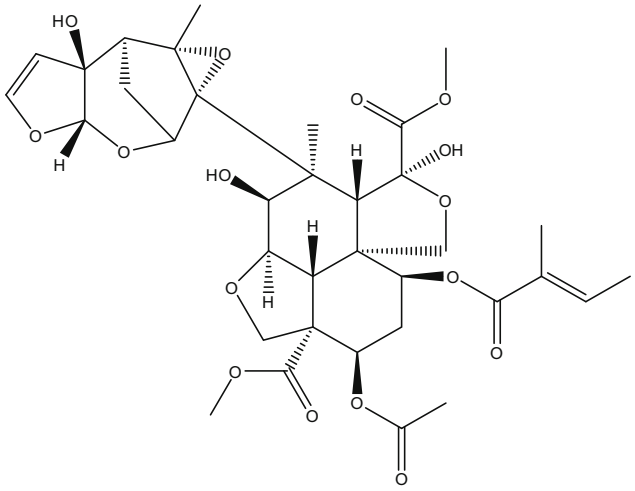

Figure 2: Azadirachtin chemical structure.

and ferric iron. As a result, it is commonly referred to as iron II and III oxide. There are three types of iron oxides found in nature: maghemite, magnetite, and hematite [25]. The hexagonal unit cell of hematite contains only octahedral coordinated Fe^{3+} atoms (corundum structure), whereas the cubic unit cell of magnetite contains both octahedral and tetrahedral coordinated Fe^{3+} atoms (the defect spinel structure) [26].

Due to its relatively low level poisonousness, new super-paramagnetic behaviour, good chemical constancy, and potent coat functionalisation with beneficial molecules to bind various biological ligands, magnetic iron oxide (Fe_3O_4) NPs have attracted amplified consideration in the biomedical commerce [25–27]. Fe_3O_4 nanoparticles (NPs), the most conventional magnetic nanoparticles because its exceptional magnetism, biocompatibility, reduced toxicity, biodegradability, and other qualities, have drawn a lot of interest in the biomedical area, particularly for targeted drug/gene delivery systems [28–30].

Silver nanoparticles (AgNPs) have generated interest during the past few years in a number of industries, including biosensors, electrical conductivity, biomedicine, catalysis, pharmaceuticals, as well as environmental uses [31]. AgNPs are the most exciting and promising material in nanotechnology due to their high specific surface energy, which encourages surface reactivity. However, AgNP agglomeration is inevitable. Therefore, a coating of magnetite onto AgNPs is required as an appropriate supplementary medium for the immobilisation of AgNPs in order to address the issues related to parting, retrieval, and constancy of AgNPs and to prevent its agglomeration throughout the creation process.

Consequently, the combining of Fe_3O_4 NPs and AgNPs to form a single hybrid functionalised nanostructure

(Ag/Fe_3O_4 NPs) reveals a method to enable the improvement of every single component of a NP [32]. There are several physical and chemical approaches that may be used to create metal/Fe_3O_4 NPs, but they frequently call for pricey equipment, hazardous chemicals, and physical and chemical tactics that can actually affect the environment and human life [33]. Paul and co-workers synthesised Ag-Fe_2O_3 and applied them for the chemoselective reduction of nitroarenes [34], Ji and co-workers synthesised silver supported on cobalt oxide for photocatalytic oxidation of aromatic alcohols [35].

By entering bacterial biofilms, the Fe_3O_4/AgNP has previously demonstrated an improved potential bactericidal impact, acting as particularly acceptable antibacterial agents that reduce toxicity in healthy cells while also providing the ability to remove them from the media by means of a magnetic field [36–40]. Uncoated Fe_3O_4 NP oxidation and aggregation, which are accompanied by reduced magnetisation values, provide a considerable problem for several applications in the biomedical sector. A potentially useful multifunctional NP in this view is the augmentation of physical characteristics by magnetic behaviour with organic/inorganic NPs. While preventing the accumulation and oxidation of Fe_3O_4 NPs, this structure retains the qualities and advantages of each component [41]. TiO_2 rutile, on the other hand, was selected as the host of the so-formed Ag/Fe_2O_3 NPs to acquire further properties for the intended nanocomposites owing to its known bioactivity. We are aware of no information about the biosynthesis of Ag/Fe_2O_3 nanocomposites utilising acacia in the presence of tulsi and neem oils. In green chemistry, we investigate the simple and sustainable synthesis of the Ag/Fe_2O_3 hybrid using acacia as the reducing agent in bioactive oils and in conjunction with TiO_2 rutile to make the desired $Ag/Fe_2O_3/TiO_2$.

2 Materials and methods

Analytical grade silver nitrate ($AgNO_3$, >99.98%) was purchased from Sigma-Aldrich. TiO_2 rutile, sodium acetate (CH_3COONa), ethanol (C_2H_5OH, >98%), and iron(III) sulphate hydrate $Fe_2(SO_4)_3{\cdot}6H_2O$ was acquired from Sigma-Aldrich. Distilled deionised (DI) water was used to make all aqueous solutions.

2.1 $Ag/Fe_2O_3/TiO_2$ biosynthesis

For the synthesis of $Ag/Fe_2O_3/TiO_2$, prepare 90 mL of a mixture solution (1% acacia, 0.1 g $Fe(SO_4)_3{\cdot}6H_2O$, and 0.1 g $AgNO_3$, and 0.2 g TiO_2), which is blended together. Following complete homogenisation of the solution, 10 mL of tulsi or neem oil is added dropwise to the solution using a magnetic stirrer at 300 rpm and 70°C for 3 h (Scheme 1). The colour shift of the reaction system was observed and recorded visually. After the precipitate has completely formed, the solution is allowed to stand for 3 h before being centrifuged for 10 min at 4,000 rpm. To remove ionic contaminants, the precipitate is thoroughly rinsed with DI water, followed by acetone to remove any organic impurities. Before being burned at 350°C for 12–15 h, the precipitate is oven dried.

2.2 $Ag/Fe_2O_3/TiO_2$ characterisation

The measurements of the powder X-ray diffraction (XRD) patterns of the materials were made on a Holland Philips X-ray powder diffractometer using Cu K radiation (=0.1542 nm) with smattering angles (2) of 5–80. Additionally, a few samples of synthetic $Ag/Fe_2O_3/TiO_2$ NPs were generated for scanning electron microscopy (SEM) experiments by ultrasonically dispersing the NPs in ethanol, and the suspensions were then placed onto a copper grid covered in carbon. Fourier-transform infrared spectroscopy (FT-IR) spectra were obtained on a Bruker VERTEX 80 v model to investigate the functional group of materials that were analyzed using KBr disc technique on a Bruker VERTEX 80 v model while SEM was performed using a (CM30 3000Kv). The functional group of materials was investigated utilising The dynamic light scattering (DLS) method was used to characterise the size distribution of $Ag/Fe_2O_3/TiO_2$ NPs, and a computerised inspection system (MALVERN Zen3600) with DTS® (nano) software was used. Using a Varian Cary 50 UV-vis spectrophotometer, UV-Vis studies were performed. Spectra between 350 and 800 nm were captured.

3 Results and discussion

In this investigation on the production of $Ag/Fe_2O_3/TiO_2$, the oils of neem and tulsi were selected and used. Neem and tulsi oils, which can act as a dropping and stabilising mediator in the synthesis of $Ag/Fe_2O_3/TiO_2$ nanocomposite, are the main ingredients in this process, which aim to offer a clean, ecologically friendly approach of producing nanomaterials.

Fe $(SO_4)_3{\cdot}6H_2O$ and $AgNO_3$ were used as precursors in the synthesis of $Ag/Fe_2O_3/TiO_2$ by adding them to neem and tulsi until a gradual change in reaction colour was seen.

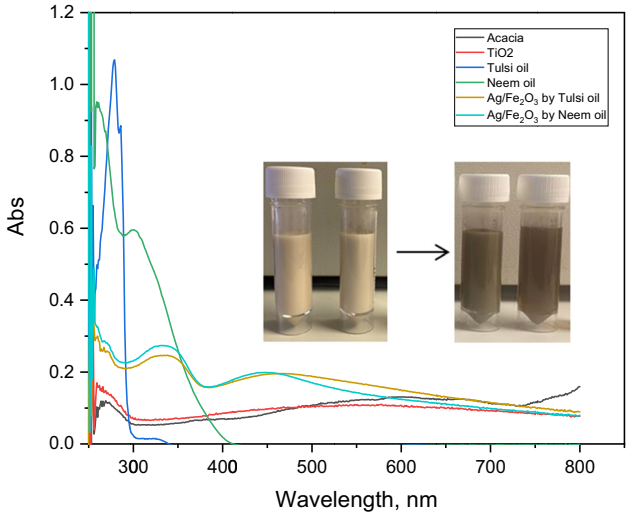

Figure 3: Colour change and UV-Vis absorption spectra of $Ag/Fe_2O_3/TiO_2$ nano-composite synthesis by tulsi and neem oils.

The reaction mixture's colour changed from white to brown after 3 h of incubation at 70°C (Figure 3). Figure 3 shows the Ag/Fe_2O_3 nanocomposite's UV-Vis spectra after 3 h, which were measured in the 300–800 nm region. The large peak created at 320 nm, as shown in the UV-Vis spectra, served as a signal to recognise the development of $Ag/Fe_2O_3/TiO_2$ nanocomposite. Similar to this, Berastegui et al.'s UV-Vis investigations of $AgFeO_2$ NPs exhibited strong absorptions between 300 and 650 nm [42]. The increase in absorbance at 320 nm was brought on by the addition of $Ag/Fe_2O_3/TiO_2$ nanocomposite (Figure 3).

The physical characteristics of the bioactive components in tulsi and neem oils, as well as potential biochemical changes brought on by the production of $Ag/Fe_2O_3/TiO_2$, were examined using FT-IR spectroscopic examination with a spectrum range of 400–4,000 cm^{-1}, as shown in Figure 4. The hydroxyl and phenolic groups in tulsi and neem oils were found to vibrate in a wide range between 3,367.9 and 3,216.9 cm^{-1} [43]. The bands located at 2,918.5 cm^{-1} and 2,850.6 cm^{-1} belong to the –CH group. The sharp peaks on 1,728.7 cm^{-1} point to the presence of C–O in the ester group. The peak on 1,603.8 cm^{-1} signifies the existence of NH amine. The peak value of 1,008 cm^{-1} provided by FT-IR analysis, which further supports the presence of practical groups like carboxylic acid and ether, is used in this context. The bioactive substances in tulsi and neem oils are used to change ions into the proper metal forms. Additionally, these phytochemicals have highly sensitive hydroxyl groups that produce hydrogen and reduce free radicals by doing so.

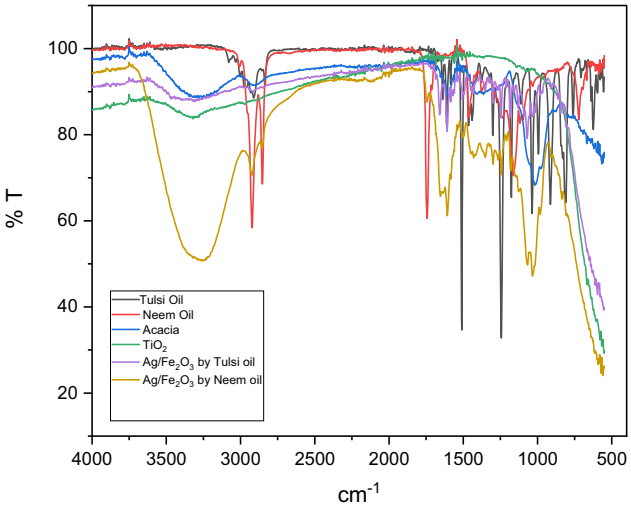

Figure 4: FTIR spectral analysis of neem and tulsi oils, and $Ag/Fe_2O_3/TiO_2$ nanocomposite.

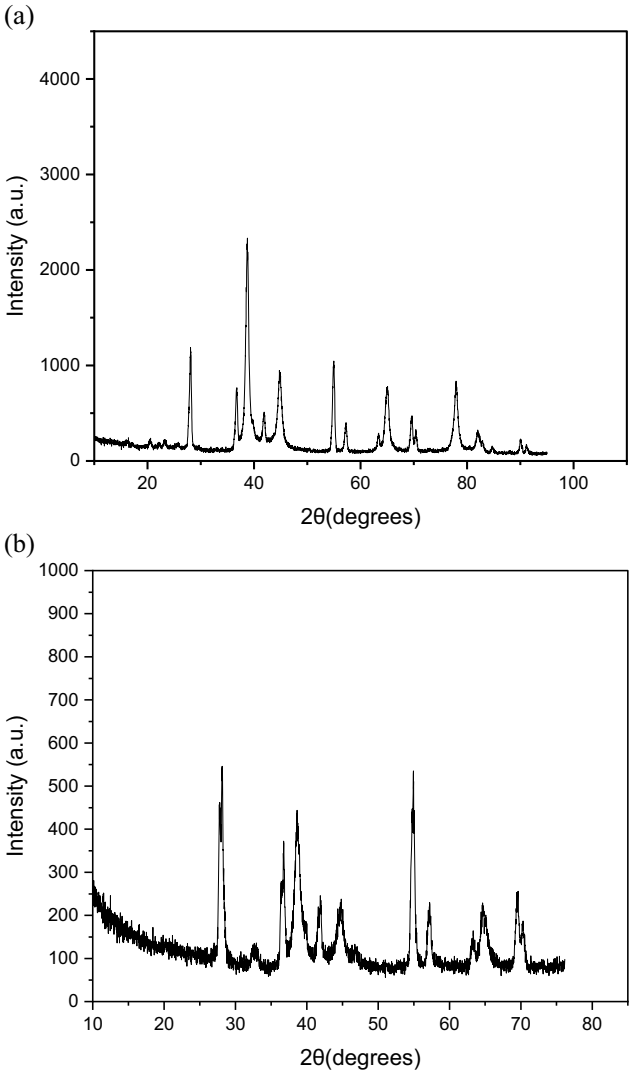

Figure 5: XRD of the synthesised $Ag/Fe_2O_3/TiO_2$ by (a) tulsi oil and (b) neem oil.

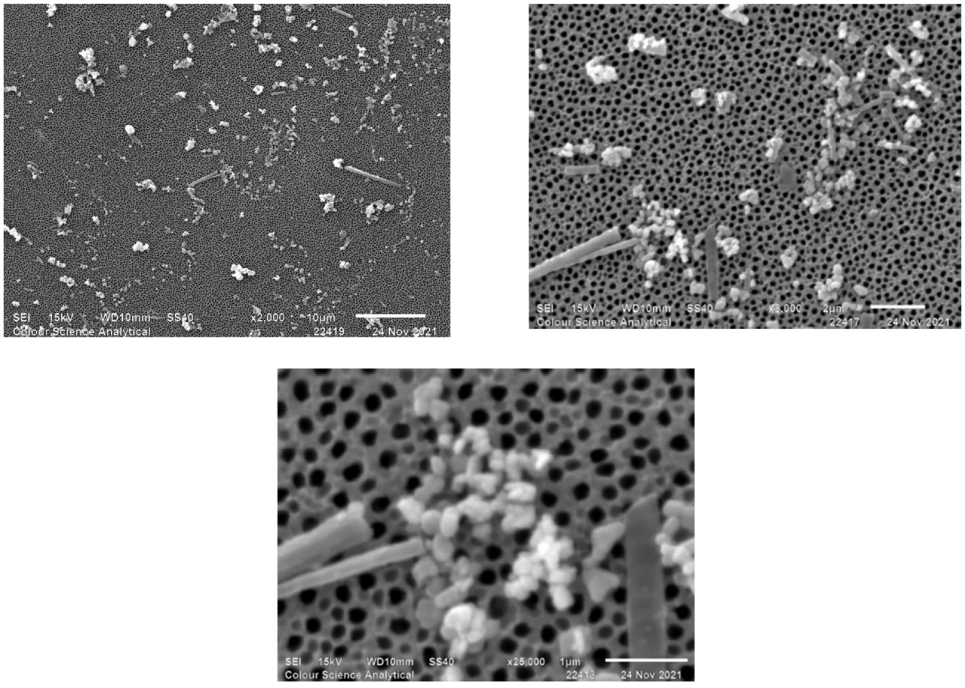

Figure 6: SEM of the synthesised Ag/Fe_2O_3/TiO_2 by tulsi oil.

The results provide credence to the hypothesis that these phytochemicals are involved in the bio-reduction process that generates nanomaterials [44]. According to the IR spectra of Ag/Fe_2O_3/TiO_2 (Figure 4), changes during Ag/Fe_2O_3/TiO_2 formation, including redox of phytochemicals, can be blamed for the suppression of aliphatic molecules. Additionally, IR measurements showed that chemical groups from the extract were attached to the Ag/Fe_2O_3/TiO_2 layer, proving that the use of tulsi and neem oils as stabilisers aided in the production of nanocomposite materials. The presence of peaks at 611.4 and

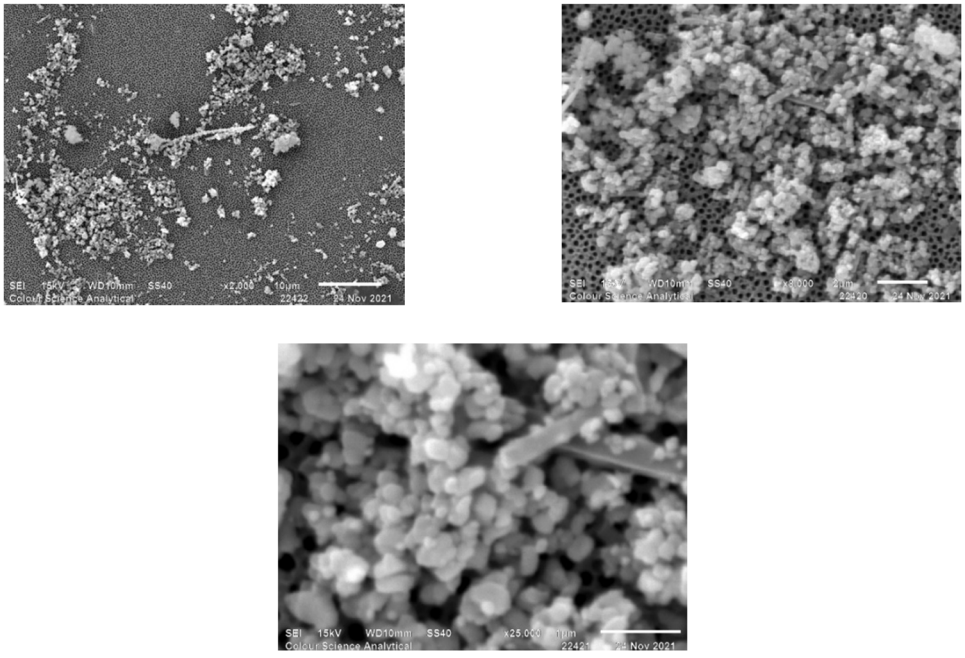

Figure 7: SEM of the synthesised Ag/Fe_2O_3/TiO_2 by neem oil.

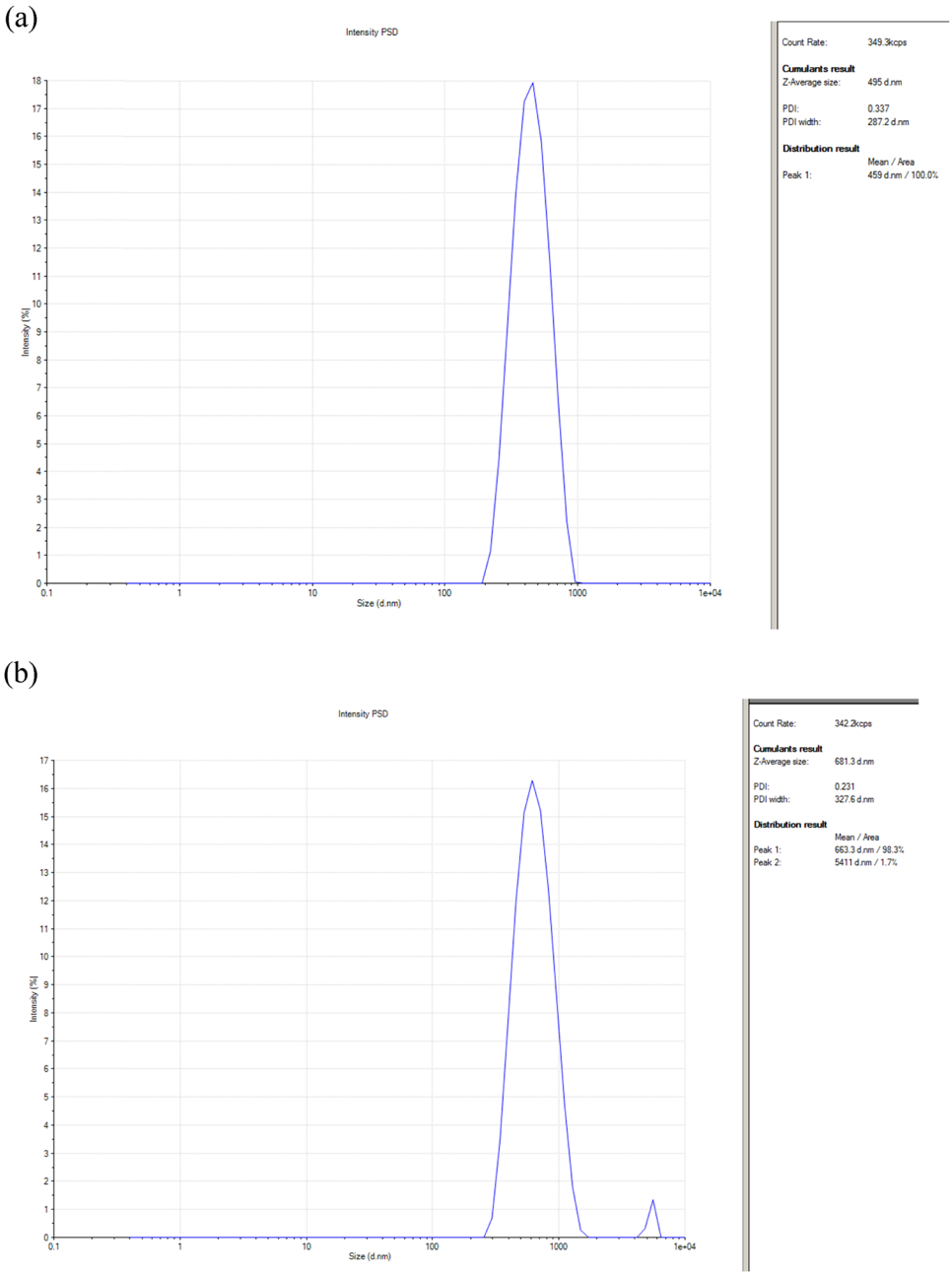

Figure 8: DLS of the synthesised $Ag/Fe_2O_3/TiO_2$ by (a) tulsi oil and (b) neem oil.

Table 1: DLS of the synthesised $Ag/Fe_2O_3/TiO_2$ by tulsi and neem oils

Sample reference	*Z*-Average (*d*·nm)	PDI	PDI width (*d*·nm)	Mean value/ area (*d*·nm) (%)
Tulsi oil	495.0	0.337	287.2	459/100
Neem oil	681.3	0.231	327.6	Peak 1/98.3 663.3 Peak 2/1.7 5,411

561.4 cm^{-1}, respectively, in (Figure 4) may be explained by the bending vibration of AgO and FeO interactions in $Ag/Fe_2O_3/TiO_2$.

XRD analysis was used to verify the $Ag/Fe_2O_3/TiO_2$ NPs' crystalline structure, as shown in Figure 5. The diffraction peaks of TiO_2 rutile at 2θ = 27.3°, 36.0°, 41.1°, 54.2°, 62.7°, and 69.0° are related to the (110), (101), (111), (211), (002), and (112) reticular planes of rutile [45]. Characteristic diffraction peaks due to AgNPs at 2θ values of 38.32, 44.54, 64.61, 77.54, and 81.68 corresponding to (111), (200), (220), (311), and (222) planes of silver is observed (JCPDS, silver file

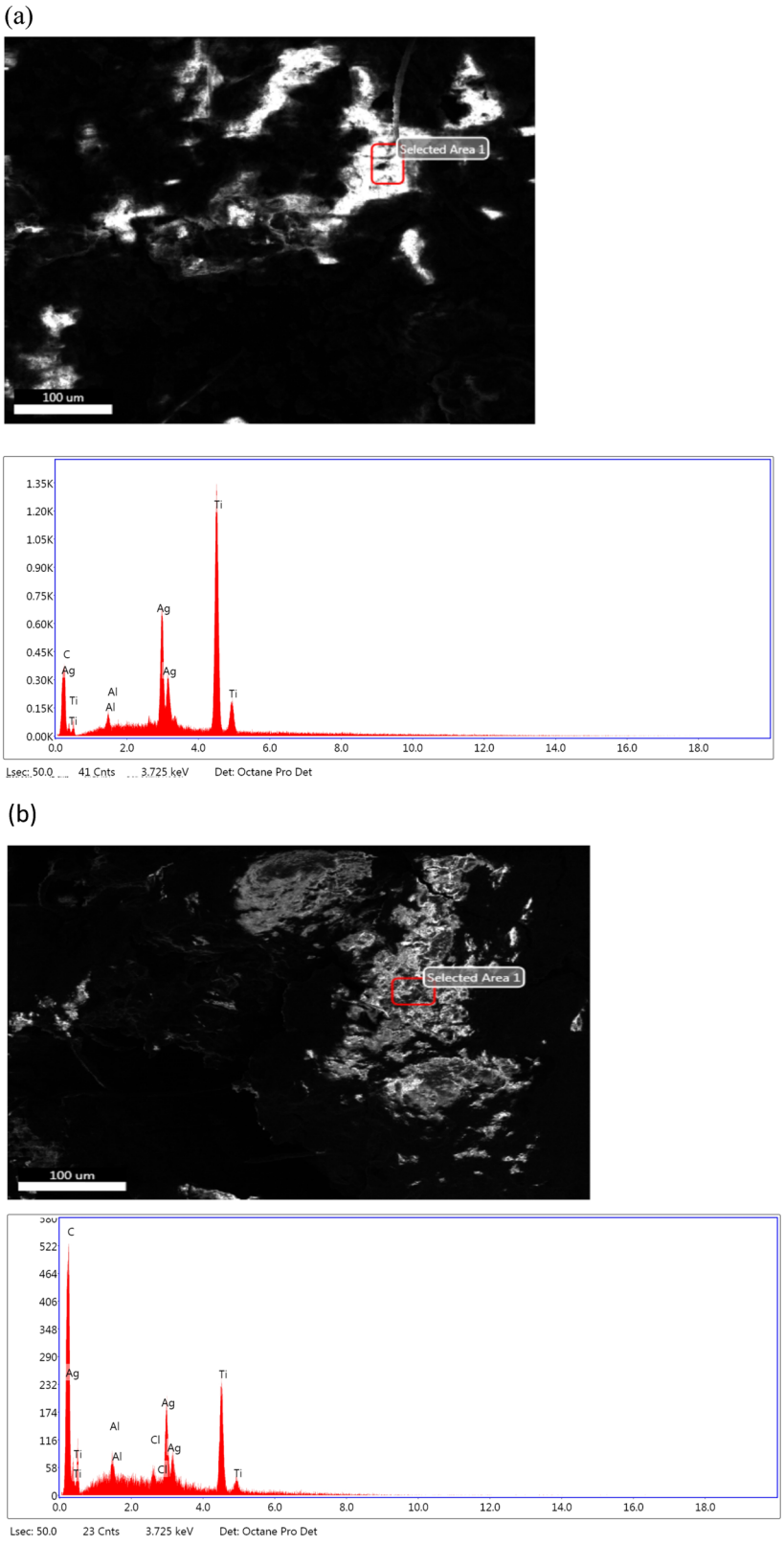

Figure 9: EDX analysis (a) Ag/Fe_2O_3/TiO_2 tulsi oil and (b) Ag/Fe_2O_3/TiO_2 neem oil.

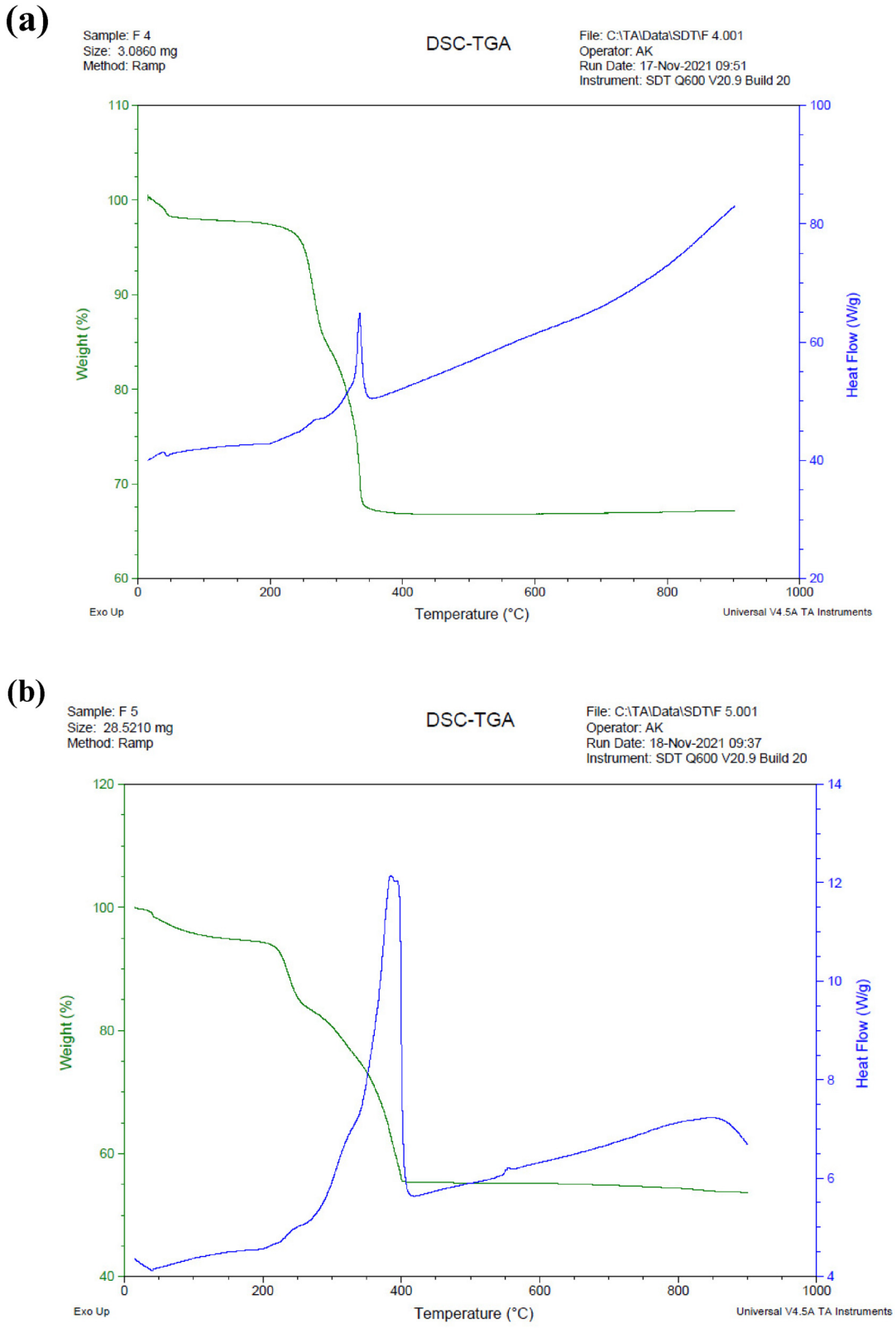

Figure 10: TGA of (a) $Ag/Fe_2O_3/TiO_2$ tulsi oil and (b) $Ag/Fe_2O_3/TiO_2$ neem oil.

No. 04–0783). On the other hand, Fe_2O_3 diffraction peaks appear partially overlapped with those of AgNPs and TiO_2 and can be observed at 35.7, 53.1, 57.1, and 62.7 and attributed to the planes of (311), (422), (511), and (440) from the cubic structure of γ-Fe_2O_3 NPs (JCPDS, No. 04-0755).

The SEM is the method that is most frequently used to determine the morphological characteristics and sizes of manufactured nanostructures. As observed in the SEM images (Figures 6 and 7), the Ag/Fe_2O_3/TiO_2 nanocomposites are produced in a spherical shape, with an average size range of 25–174 nm. The bright circular spots revealed the nanocomposite planes and the degree of crystallinity of the Ag/Fe_2O_3/TiO_2 particles made up of neem and tulsi oils (Figures 6 and 7). DLS analysis was used to measure the average diameter of the Ag/Fe_2O_3/TiO_2 nanocomposite. The bulk diameter of the Ag/Fe_2O_3 nanocomposite is 270.9 nm. However, the metal core (Ag and Fe) of the Ag/Fe_2O_3/TiO_2 nanocomposite as well as the biomaterials (organic chemicals related as stabilisers) deposited by neem and tulsi oils on the Ag/Fe_2O_3/TiO_2 surface change the size estimated by DLS [46] (Figure 8 and Table 1).

The Ag/Fe_2O_3/TiO_2 nanocomposite surface had components efficiently deposited on it, according to an energy-dispersive X-ray (EDX) analysis (Figure 9). The Ag/Fe_2O_3/TiO_2 nanocomposite was found to include multiple distinct peaks in the EDX spectra which were linked to the oxygen, silver, iron, and carbon constituents (Figure 9). The development of an extremely pure Ag/Fe_2O_3/TiO_2 nanocomposite with no extra impurity-related peaks was further demonstrated by EDX spectra. The SEM image and EDX spectra of the nanocomposite showed that the Ag/Fe_2O_3/TiO_2 nanostructures were evenly distributed throughout the neem and tulsi. In addition, the composition of Ag and Fe in Ag/Fe_2O_3/TiO_2 was determined by elemental EDX mapping. Figure 9 shows the charting of Fe, Ag, O, and C. As stated by the EDX fundamental analysis in the Fe, Ag, O, and C component charting imageries of Ag/Fe_2O_3/TiO_2 (Figure 9), both Ag and Fe were uniformly distributed throughout the sample [47].

TGA studies are performed by heating the materials in air to 600°C (Figure 10) in order to determine the thermal stability.

Figure 10(a and b) depicts the Ag/Fe_2O_3/TiO_2 nanocomposite TGA curves produced by tulsi and neem oils. The greatest loss of weight (65%) at the range of temperature between 170°C and 525°C may be attributed to the pyrolysis of the labile oxygen-comprising clusters in the forms of CO_2, CO, and vapour. The loss of weight of approximately 5% at the temperatures between 100°C and 170°C may be because of the water molecules elimination and it was confined inside the GO. When the Ag/Fe_2O_3/TiO_2 nanocomposite sample was heated to 800°C at an incremental rate of 10°C·min^{-1}, there was only a 17% total weight loss. This weight loss is due to the removal of remaining Ag/Fe_2O_3/TiO_2 nanocomposite oxygen-containing groups from tulsi and neem oils.

Although the quantitative findings from this approach are not as precise as those from atomic absorption analysis, they are nevertheless reliable when comparing the amounts of silver in the samples.

4 Conclusion

One of the most fascinating subjects in the realm of nanotechnology is the green production of nanomaterials. In this sense, recent years have seen advancements in biosynthesis utilising medicinal plant oils. Tulsi and neem oils were used in this study as reducing agents to change the Ag0 cation in $AgNO_3$ solution to Ag0. Ag/Fe_2O_3/TiO_2 NPs were created as a result of the interaction between $AgNO_3$ solution and acacia in the presence of tulsi and neem oils. The effective synthesis of Ag/Fe_2O_3/TiO_2 NPs was validated by a variety of characterisation techniques, including XRD, SEM, FT-IR, DLS, and UV-vis spectroscopy. The outcome of the DLS study and the SEM picture indicated that the average particle size was 28 nm. Similarly, SEM scans showed that Ag/Fe_2O_3/TiO_2 NPs had spherical shapes. The FT-IR data also showed that tulsi and neem oils were used as surfactants and capping agents to regulate the form and size of these NPs. Last but not least, this technique may be used to produce various kinds of metal NPs on a big scale and remove a lot of harmful chemical reagents used in manufacturing nanomaterials. Future work would be the potential application of the new materials made, and the outcome of this work will be published elsewhere.

Acknowledgements: The authors extend their appreciation to the King Deanship of Scientific Research at Khalid University for funding this work through a large group Research Project under grant number RGP2/143/44.

Funding information: Khalid University for funding this work through a large group Research Project under grant number RGP2/143/44.

Author contributions: Fatimah Ali M. Al-Zahrani: writing – original draft, writing – review and editing, methodology, and formal analysis; project administration; Reda M. El-Shishtawy: writing – original draft, writing – review and editing, methodology, and formal analysis

Conflict of interest: Authors state no conflict of interest.

Data availability statement: The datasets generated during and/or analysed during the current study are available from the corresponding author on reasonable request.

References

[1] Al-Zahrani FAM, AL-Zahrani NA, Al-Ghamdi SN, Lin L, Salem SS, El-Shishtawy RM, et al. Synthesis of Ag/Fe_2O_3 nanocomposite from essential oil of ginger via green method and its bactericidal activity. Biomass Convers Biorefin. 2022;12(10):1–9.

[2] Al-Zahrani F, Salem SS, Al-Ghamdi HA, Nhari LM, Lin L, El-Shishtawy RM. Green synthesis and antibacterial activity of Ag/Fe_2O_3 nanocomposite using Buddleja lindleyana extract. Bioengineering. 2022;9(9):452.

[3] Paul B, Bhuyan B, Dhar Purkayastha D, Dey M, Dhar SS. Green synthesis of gold nanoparticles using *Pogestemon benghalensis* (B) O. *Ktz*. leaf extract and studies of their photocatalytic activity in degradation of methylene blue. Mater Lett. 2015;148:37–40.

[4] Koech RK, Olanrewaju YA, Ichwani R, Kigozi M, Oyewole DO, Oyelade OV, et al. Effects of polyethylene oxide particles on the photo-physical properties and stability of FA-rich perovskite solar cells. Sci Rep. 2022;12(1):12860.

[5] Anderson SD, Gwenin VV, Gwenin CD. Magnetic functionalized nanoparticles for biomedical, drug delivery and imaging applications. Nanoscale Res Lett. 2019;14:1–16.

[6] Comanescu C. Magnetic nanoparticles: Current advances in nanomedicine, drug delivery and MRI. Chemistry. 2022;4(3):872–930.

[7] Varadavenkatesan T, Pai S, Vinayagam R, Selvaraj R. Characterization of silver nano-spheres synthesized using the extract of Arachis hypogaea nuts and their catalytic potential to degrade dyes. Mater Chem Phys. 2021;272:125017.

[8] Bhole R, Gonsalves D, Murugesan G, Narasimhan MK, Srinivasan NR, Dave N, et al. Superparamagnetic spherical magnetite nanoparticles: synthesis, characterization and catalytic potential. Appl Nanosci. 2023;13(9):6003–14.

[9] Shet VB, Kumar PS, Vinayagam R, Selvaraj R, Vibha C, Rao S, et al. Cocoa pod shell mediated silver nanoparticles synthesis, characterization, and their application as nanocatalyst and antifungal agent. Appl Nanosci. 2023;13(6):4235–45.

[10] Agarwal P, Nagesh L. Evaluation of the antimicrobial activity of various concentrations of Tulsi (Ocimum sanctum) extract against Streptococcus mutans: An in vitro study. Indian J Dental Res. 2010;21(3):357–9.

[11] Pandey G, Madhuri S. Pharmacological activities of Ocimum sanctum (tulsi): a review. Int J Pharm Sci Rev Res. 2010;5(1):61–6.

[12] Baliga MS, Jimmy R, Thilakchand KR, Sunitha V, Bhat NR, Saldanha E, et al. Ocimum sanctum L (Holy Basil or Tulsi) and its phytochemicals in the prevention and treatment of cancer. Nutr cancer. 2013;65(sup1):26–35.

[13] Borah R, Biswas S. Tulsi (Ocimum sanctum), excellent source of phytochemicals. Int J Environ Agric Biotechnol. 2018;3(5):265258.

[14] Verma S. Chemical constituents and pharmacological action of Ocimum sanctum (Indian holy basil-Tulsi). J Phytopharmacol. 2016;5(5):205–7.

[15] Yamani HA, Pang EC, Mantri N, Deighton MA. Antimicrobial activity of Tulsi (Ocimum tenuiflorum) essential oil and their major constituents against three species of bacteria. Front Microbiol. 2016;7:681.

[16] Mohan L, Amberkar M, Kumari M. Ocimum sanctum linn (TULSI) - an overview. Int J Pharm Sci Rev Res. 2011;7(1):51–3.

[17] Rahmani A, Almatroudi A, Alrumaihi F, Khan A. Pharmacological and therapeutic potential of neem (Azadirachta indica). Pharmacogn Rev. 2018;12(24):250–5.

[18] Saha S, Singh D, Rangari S, Negi L, Banerjee T, Dash S, et al. Extraction optimization of neem bioactives from neem seed kernel by ultrasonic assisted extraction and profiling by UPLC-QTOF-ESI-MS. Sustain Chem Pharm. 2022;29:100747.

[19] Campos EV, de Oliveira JL, Pascoli M, de Lima R, Fraceto LF. Neem oil and crop protection: from now to the future. Front plant Sci. 2016;7:1494.

[20] Roy A, Saraf S. Limonoids: overview of significant bioactive triterpenes distributed in plants kingdom. Biol Pharm Bull. 2006;29(2):191–201.

[21] Igbo UE, Ishola RO, Siedoks AO, Akubueze EU, Isiba VI, Igwe CC. Comparative study of physicochemical and fatty acid profiles of oils from under utilised nigerian oil seeds. The Pharmaceutical and Chemical Journal. 2019;6(5):103–9

[22] Kumari P, Geat N, Maurya S, Meena S. Neem: Role in leaf spot disease management: A review. J Pharmacogn Phytochem. 2020;9(1):1995–2000.

[23] Khanam Z, Al-Yousef HM, Singh O, Bhat IU. Neem oil. Green pesticides handbook: Essential oils for pest control. New York, NY, USA: CRC Press; 2017. p. 377.

[24] Islas JF, Acosta E, G-Buentello Z, Delgado-Gallegos JL, Moreno-Treviño MG, Escalante B, et al. An overview of Neem (Azadirachta indica) and its potential impact on health. J Funct Foods. 2020;74:104171.

[25] Pourbahar N, Alamdar SS. Phytofabrication, and characterization of Ag/Fe_3O_4 nanocomposite from rosa canina plant extracts using a green method. Asian J Green Chem. 2023;7:9–16.

[26] Taha AB, Essa MS, Chiad BT. Spectroscopic study of iron oxide nanoparticles synthesized via hydrothermal method. Chem Methodol. 2022;6(12):977–84.

[27] Fadli A, Amri A, Sari EO, Sukoco S, Saprudin D. Superparamagnetic nanoparticles with mesoporous structure prepared through hydrothermal technique. In Materials science forum. 2020;1000(1):203–9.

[28] Liu M, Ye Y, Ye J, Gao T, Wang D, Chen G, et al. Recent advances of magnetite (Fe_3O_4)-based magnetic materials in catalytic applications. Magnetochemistry. 2023;9(4):110.

[29] Noh J, Osman OI, Aziz SG, Winget P, Brédas JL. Magnetite Fe_3O_4 (111) surfaces: impact of defects on structure, stability, and electronic properties. Chem Mater. 2015;27(17):5856–67.

[30] Jain S, Shah J, Dhakate SR, Gupta G, Sharma C, Kotnala RK. Environment-friendly mesoporous magnetite nanoparticles-based hydroelectric cell. J Phys Chem C. 2018;122(11):5908–16.

[31] Ravichandran R, Annamalai K, Annamalai A, Elumalai S. Solid state–Green construction of starch-beaded Fe_3O_4@ Ag nanocomposite as superior redox catalyst. Colloids Surf A: Physicochem Eng Asp. 2023;664:131117.

[32] Elhouderi ZA, Beesley DP, Nguyen TT, Lai P, Sheehan K, Trudel S, et al. Synthesis, characterization, and application of Fe_3O_4/Ag magnetic composites for mercury removal from water. Mater Res Express. 2016;3(4):045013.

[33] Qi C-C, Zheng J-B. Synthesis of Fe_3O_4–Ag nanocomposites and their application to enzymeless hydrogen peroxide detection. Chem Pap. 2016;70(4):404–11.
[34] Paul B, Purkayastha DD, Dhar SS, Das S, Haldar S. Facile one-pot strategy to prepare Ag/Fe_2O_3 decorated reduced graphene oxide nanocomposite and its catalytic application in chemoselective reduction of nitroarenes. J Alloy Compd. 2016;681:316–23.
[35] Ji X, Chen Y, Paul B, Vadivel S. Photocatalytic oxidation of aromatic alcohols over silver supported on cobalt oxide nanostructured catalyst. J Alloy Compd. 2019;783:583–92.
[36] Katz E. Synthesis, properties and applications of magnetic nanoparticles and nanowires – A brief introduction. Magnetochemistry. 2019;5(4):61.
[37] Pang Y, Wang C, Wang J, Sun Z, Xiao R, Wang S. Fe_3O_4@Ag magnetic nanoparticles for microRNA capture and duplex-specific nuclease signal amplification based SERS detection in cancer cells. Biosens Bioelectron. 2016;79:574–80.
[38] Chen T, Geng Y, Wan H, Xu Y, Zhou Y, Kong X, et al. Facile preparation of Fe_3O_4/Ag/RGO reusable ternary nanocomposite and its versatile application as catalyst and antibacterial agent. J Alloy Compd. 2021;876:160153.
[39] Nguyen-Tri P, Nguyen VT, Nguyen TA. Biological activity and nanostructuration of Fe_3O_4-Ag/high density polyethylene nanocomposites. J Compos Sci. 2019;3(2):34.
[40] Venkateswarlu S, Natesh Kumar B, Prathima B, Anitha K, Jyothi NVV. A novel green synthesis of Fe_3O_4-Ag core shell recyclable nanoparticles using Vitis vinifera stem extract and its enhanced antibacterial performance. Phys B: Condens Matter. 2015;457:30–5.
[41] Thu TV, Ko PJ, Nguyen TV, Vinh NT, Khai DM, Lu LT. Green synthesis of reduced graphene oxide/Fe_3O_4/Ag ternary nanohybrid and its application as magnetically recoverable catalyst in the reduction of 4-nitrophenol. Appl Organomet Chem. 2017;31(11):e3781.
[42] Berastegui P, Tai C-W, Valvo M. Electrochemical reactions of $AgFeO_2$ as negative electrode in Li-and Na-ion batteries. J Power Sources. 2018;401:386–96.
[43] Kaloti M, Kumar A. Synthesis of chitosan-mediated silver coated γ-Fe_2O_3 (Ag− γ-Fe_2O_3@Cs) superparamagnetic binary nanohybrids for multifunctional applications. J Phys Chem C. 2016;120(31):17627–44.
[44] Kulkarni S, Jadhav M, Raikar P, Barretto DA, Vootla SK, Raikar US. Green synthesized multifunctional Ag@Fe_2O_3 nanocomposites for effective antibacterial, antifungal and anticancer properties. N J Chem. 2017;41(17):9513–20.
[45] Du J, Sun H. Polymer/TiO_2 hybrid vesicles for excellent UV screening and effective encapsulation of antioxidant agents. ACS Appl Mater Interfaces. 2014;6:13535–41.
[46] Mirzaei A, Janghorban K, Hashemi B, Bonavita A, Bonyani M, Leonardi SG, et al. Synthesis, characterization and gas sensing properties of Ag@ α-Fe_2O_3 core–shell nanocomposites. Nanomaterials. 2015;5(2):737–49.
[47] Liu J, Wu W, Tian Q, Dai Z, Wu Z, Xiao X, et al. Anchoring of $Ag_6Si_2O_7$ nanoparticles on α-Fe_2O_3 short nanotubes as a Z-scheme photocatalyst for improving their photocatalytic performances. Dalton Trans. 2016;45(32):12745–55.